This is a Just Accepted version, keep updated with https://doi.org/10.26599/LLES.2026.9660022

Research Article

Multi-hazard performance of novel ductile beam-column connections under fire and seismic loading

Yan Su, Yu Liu✉, Bohan Sun, Yize Chai, Yan Jin

School of Environment and Architecture, University of Shanghai for Science and Technology, Shanghai 200093, China.

✉ Address correspondence to Yu Liu, liuyu651020@usst.edu.cn

Received: 23 June 2026; Revised: 06 August 2026; Accepted: 06 September 2026

© The Author(s) 2026. This is an open access article under the terms of the Creative Commons Attribution 4.0 International License (CC BY 4.0, http://creativecommons.org/licenses/by/4.0/).

ABSTRACT

Connections play a critical role in governing the robustness of steel structures under extreme loading conditions. This study proposes three novel beam–column connection prototypes incorporating semi-elliptical ductile components to enhance structural performance under multi-hazard scenarios. Finite element models are developed in Abaqus to investigate the behaviour of the proposed connections throughout the full fire process, including heating and cooling, as well as under cyclic loading representative of seismic actions. Temperature-dependent material behaviour is incorporated using a user-defined subroutine. The results show that all three prototypes exhibit stable behaviour during fire, accommodating the transition from compression induced by thermal expansion to tension governed by catenary action. The ductile components enable controlled deformation and effective force redistribution. Under cyclic loading, stable hysteretic responses are observed, indicating reliable energy dissipation and ductility. Overall, the proposed connections provide an effective approach to improving both fire resistance and seismic performance, highlighting the importance of controlled deformability in enhancing structural resilience under multi-hazard conditions.

Keywords: fire; connections; ductility; earthquake

Just Accepted

1. Introduction

Connections ensure the integrity and stability of steel and steel–concrete composite frames by providing the primary load-transfer paths between structural members. As key force-transmitting components, beam–column connections largely govern the global structural response, particularly under extreme loading conditions. Evidence from past structural failures has shown that damage frequently initiates in connection regions, which can subsequently trigger progressive collapse.

Connections have traditionally been assumed to possess adequate fire resistance, partly because their temperatures are often lower than those of adjacent members. However, observations from the collapse of the World Trade Centre buildings [1] and the Cardington full-scale fire tests [2] have demonstrated that this assumption is not always valid, and that connection failure can play a critical role in structural collapse during fire. In current design practice, connections are generally designed for ambient conditions, where loading scenarios are relatively well defined. Under fire, however, their behaviour becomes considerably more complex due to temperature-induced deformation of beams. During the heating phase, restrained thermal expansion generates compressive forces in the connections. At higher temperatures, the development of catenary action leads to significant tensile forces. During cooling, thermal contraction combined with the recovery of material stiffness can further increase tensile demands, in some cases exceeding those developed during heating. Despite this, the response of connections during the cooling phase remains insufficiently understood. Previous studies have shown that connections may experience substantial tensile forces throughout the fire process. Qiang [3], for example, investigated the fire and post-fire performance of high-strength steel end-plate connections through experimental and numerical analyses, and demonstrated that post-fire behaviour is strongly dependent on connection configuration, with significant tensile forces developing during cooling. Nevertheless, most existing studies have focused on conventional connection forms and have primarily examined load-bearing capacity. Comparatively little attention has been given to deformation capacity and ductility over the full fire history. In practice, conventional connections often lack sufficient deformability to accommodate restrained thermal expansion, catenary action, and the associated large rotations.

To address these limitations, the authors previously proposed a ductile connection with enhanced axial and rotational deformability [3-7]. Component-based models for both bare-steel and composite configurations were developed and implemented in Vulcan [4-7] , and applied in a series of frame

Just Accepted

analyses incorporating different connection types [5, 7]. The results showed that the proposed connection can significantly reduce the net axial force compared with conventional connections, while also achieving higher failure temperatures. These findings highlight the importance of deformability in improving connection performance under fire.

Connection deficiencies are also evident under seismic loading. Damage observed in steel frames during the Northridge and Kobe earthquakes [8] was largely associated with brittle fracture of beam–column connections, indicating that the expected strength and stiffness could not be maintained under cyclic loading. Conventional seismic-resistant connections are prone to low-cycle fatigue in bolts or weld fracture, reflecting limited energy dissipation capacity and rotational ductility. In response, a range of innovative connection details have been proposed to improve seismic performance, often through energy dissipation or replaceable components. For example, He and Chen[9] developed a replaceable composite beam connection in which damage is concentrated in sacrificial angle components, allowing structural stiffness and strength to be restored after replacement. Tagawa et al. [10] introduced a connection incorporating rod dampers to dissipate seismic energy, while Wang et al. [11] proposed a bolted connection with replaceable low-yield components designed to concentrate plastic deformation and protect primary structural members.

While these developments have improved performance under individual hazards, most studies have focused on either fire or earthquake loading in isolation. The behaviour of connections under sequential or combined multi-hazard scenarios remains insufficiently explored. Recent studies suggest that connection details optimised for a single hazard may not perform adequately under other hazards, and may even exhibit increased vulnerability [12, 13]. Against this background, this paper develops three connection types: pinned, semi-rigid, and rigid, based on the previously proposed ductile connection concept. The three configurations share consistent key parameters, including plate thickness and the geometry of the ductile components, enabling direct comparison of their behaviour. Finite element models are established in Abaqus to investigate their response under fire and seismic conditions. A user-defined subroutine (VUSDFLD) is implemented to account for temperature-dependent material behaviour during heating, cooling, and post-fire stages. The modelling approach is validated against available experimental results. The results show that all three connection types maintain stable behaviour under both fire and seismic loading, with sufficient deformability to accommodate large rotations and force redistribution. This enables a

Just Accepted

reduction in force demand while preserving load-transfer capacity throughout the loading process. The proposed connections therefore provide a consistent and effective solution for improving structural robustness under multi-hazard conditions.

2. Design of the novel ductile connections

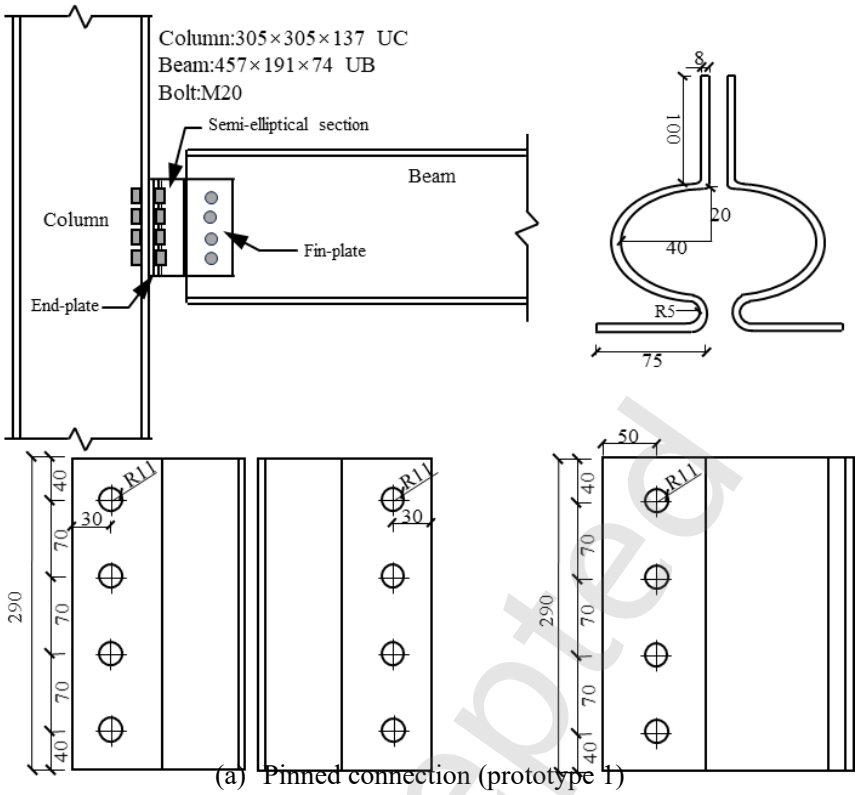
To improve the performance of beam-to-column connections under multi-hazard conditions, three novel connection systems are developed, as shown in Figure 1. The proposed configurations are based on a unified design concept, in which semi-elliptical ductile components are integrated with different load-transfer mechanisms to form pinned, semi-rigid, and rigid connections.

The key feature of the proposed connections is the incorporation of semi-elliptical ductile components in combination with either angle assemblies or flange cover plates. This configuration is intended to alleviate the localised failure commonly observed in conventional connections and to enhance axial deformability under alternating compression–tension loading. As a result, the connections are able to accommodate the full sequence of force development during fire, including compressive forces induced by restrained thermal expansion, tensile forces associated with catenary action at elevated temperatures, and additional tensile demands during cooling.

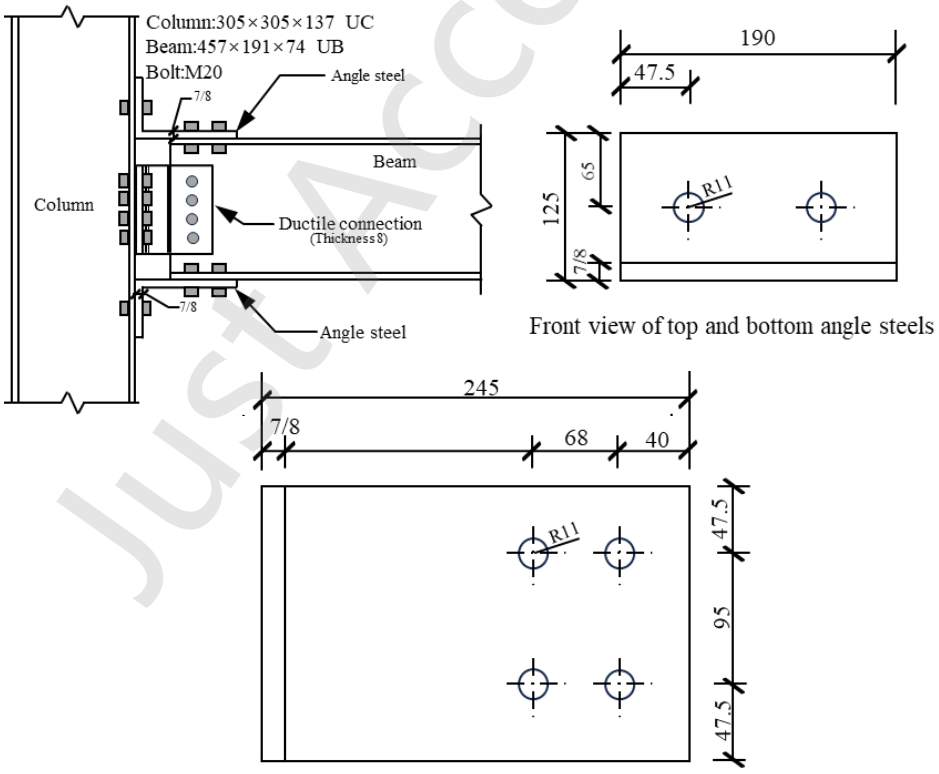
The effectiveness of the semi-elliptical ductile components in providing deformation capacity and reducing axial force has been demonstrated in the authors' previous studies [3-7, 14]. In the present design, these components also serve as ductile fuses. In the semi-rigid (prototype 2) and rigid (prototype 3) configurations, they are capable of maintaining load transfer after the failure of the angle cleats or flange cover plates, respectively. This allows the connection to retain a residual load-carrying path, thereby improving robustness under extreme loading conditions. In addition, both the ductile components and the associated angle or cover plate assemblies are detailed to facilitate replacement after damage. This enables rapid repair and restoration of structural function following extreme events, and reduces the need for intervention in primary structural members.

Just Accepted

This is a Just Accepted version, keep updated with https://doi.org/10.26599/LLES.2026.9660022



(a) Pinned connection (prototype 1)

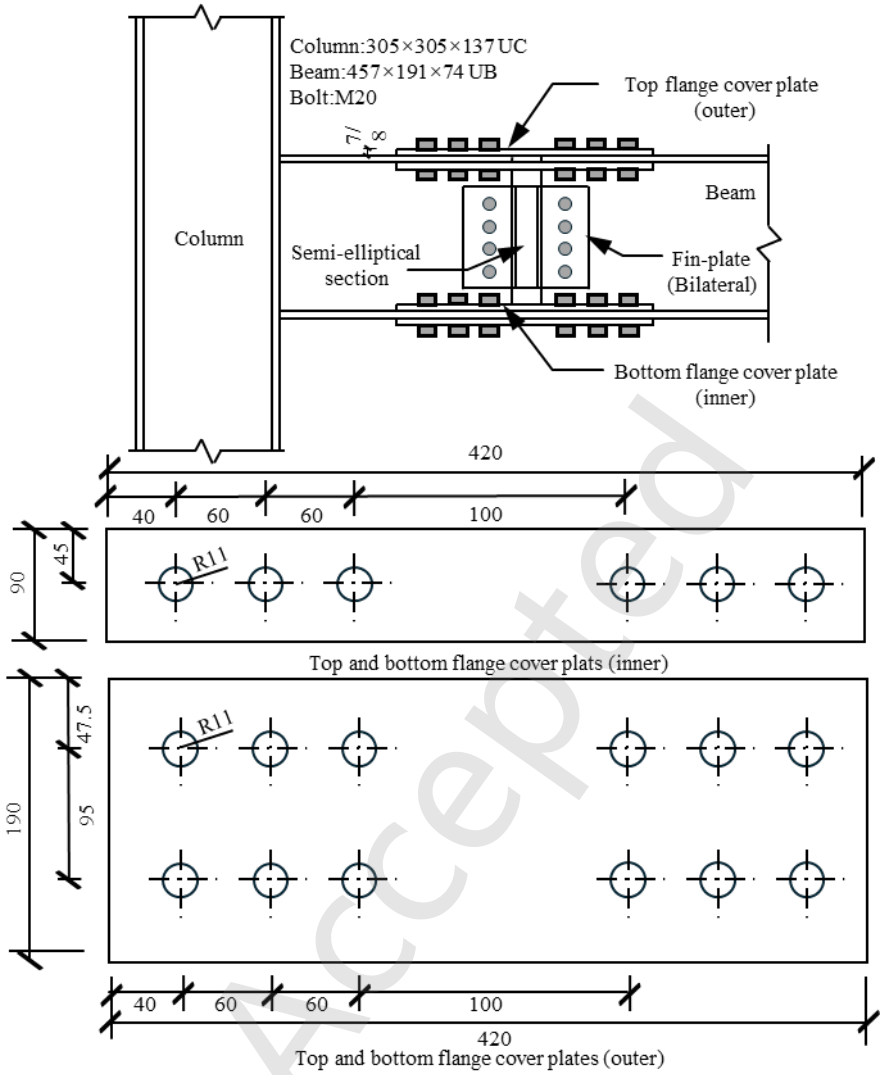


Front view of top and bottom angle steels

Plan view of top and bottom angle steels

(b) Semi-rigid connection (prototype 2)

Just Accepted



(c) Rigid connection (prototype 3)

Figure 1. Design of the ductile connections

For each prototype, the ductile component consists of two identical subassemblies. Each subassembly includes a fin plate connected to the beam web, a face plate connected to the column flange or web, and a semi-elliptical segment linking the two plates. The semi-elliptical segment acts as the primary deformable element, accommodating relative displacement between the fin plate and face plate, and providing deformation capacity under extreme loading. The geometry of the semi-elliptical segment is determined according to the ductility demand of the connected beam, which can be evaluated using the formulations proposed in the authors' previous work [3-7, 14]. The remaining design parameters, including plate thickness, bolt arrangement, and the dimensions of angle cleats and cover plates, are specified in accordance with the relevant Eurocode provisions to ensure adequate strength, stiffness, and constructability.

Just Accepted

3. Performance of connections under the entire fire process

3.1 Dimensions of the three connection prototype models

The three connection prototypes are modelled using a 457 × 191 × 74 UB beam with a span of 9000 mm and a 305 × 305 × 137 UC column with a height of 8000 mm, representing typical members used in multi-storey steel frames. The geometric configuration of each connection is defined based on the ductility demand of the connected beam, in conjunction with the design provisions of the Eurocodes. Detailed dimensions of the connection components are presented in Figure 1 and summarised in Table 1. The three prototypes are designed with consistent key parameters to ensure a meaningful comparison of their structural response.

A uniformly distributed load of 5.4 kN/m² is applied to the beam, corresponding to a load ratio of 0.4 with respect to the ambient-temperature bending resistance of the simply supported beam. The same loading condition is adopted for all three connection models to isolate the influence of connection type on structural performance.

Two fire scenarios are considered for each prototype. The first assumes a uniform temperature distribution through the beam depth, while the second accounts for a non-uniform temperature profile. The latter introduces thermal gradients and associated thermal bowing effects, allowing the influence of temperature non-uniformity on connection behaviour to be examined. The determination of the temperature distributions under the ISO 834 standard fire is described in Section 3.3.

Table 1. Dimensions of the Abaqus models (mm)

<table>
<tr><td>Beam section</td><td>457×191×74 UB</td><td>Span (mm)</td><td>9000</td><td>Load (kN/m^2)</td><td>5.4</td></tr>
<tr><td>Column section</td><td>305×305×137 UC</td><td>Height (mm)</td><td>8000</td><td>Load ratio</td><td>0.4</td></tr>
<tr><td colspan="2">Prototype 1</td><td colspan="2">Prototype 2</td><td colspan="2">Prototype 3</td></tr>
<tr><td>Long half axis</td><td>40</td><td>Top and bottom angle cleats (mm)</td><td>125×245</td><td>Top and bottom flange cover plate (outer) (mm)</td><td>190×420</td></tr>
<tr><td rowspan="2">Short half axis</td><td rowspan="2">20</td><td>Long half axis</td><td>40</td><td rowspan="2">Top and bottom flange cover plate (inner) (mm)</td><td rowspan="2">90×420</td></tr>
<tr><td>Short half axis</td><td>20</td></tr>
<tr><td>Plate thickness (mm)</td><td>8</td><td>Plate thickness (mm)</td><td>7/8</td><td>Plate thickness (mm)</td><td>7/8</td></tr>
</table>

Just Accepted

Fin-plate width (mm) × depth (mm)	100×290	Number of bolt rows connected to column	1	Fin-plate width (mm) × depth (mm)	100×290
Face-plate width (mm) × depth (mm)	75×290	Number of bolt rows connected to beam	2	Long half axis	40
Number of bolt rows	4			Short half axis	20

3.2 Material properties

3.2.1 Post-fire stage

The post-fire mechanical behaviour of structural steel is defined based on the stress–strain model proposed by Han [15], as given in Equation (1).

$$\sigma_s = \begin{cases} E_S \cdot \varepsilon_s & \varepsilon_s \le \varepsilon_{yp}(T_{\max}) \\ f_{yp}(T_{\max}) + 0.01E_s \cdot [\varepsilon_s - \varepsilon_{yp}(T_{\max})] & \varepsilon_s > \varepsilon_{yp}(T_{\max}) \end{cases} \tag{1}$$

In this equation, E_S represents the Young's modulus of steel at ambient temperature. Additionally, $\varepsilon_{yp}(T_{\max}) = f_{yp}(T_{\max}) / E_s$, where $f_{yp}(T_{\max})$ denotes the residual yield strength of steel after exposure to fire, and it can be expressed as follows:

$$\frac{f_{yp}(T_{\max})}{f_y(20°\mathrm{C})} = \begin{cases} 1 & T_{\max} \le 400°\mathrm{C} \\ 1 + 2.33\times10^{-4}(T_{\max} - 20) - 5.88\times10^{-7}(T_{\max} - 20)^2 & T_{\max} > 400°\mathrm{C} \end{cases} \tag{2}$$

3.2.2 Cooling stage

During the cooling stage, the mechanical response of steel depends on both the current temperature T and the maximum temperature previously attained $T_{\max}$. In contrast, the post-fire condition corresponds to a special case where the current temperature has returned to ambient, and the material properties depend solely on $T_{\max}$.

Following this framework, the stress–strain relationships used for the post-fire stage can be consistently extended to the cooling stage. In this study, the method proposed by Yang [16] is adopted to determine the evolution of material properties during cooling. The yield strength and yield strain at a given temperature are obtained through linear interpolation between the values corresponding to T_{max} and those at the post-fire state, as defined in Equations (3) – (6).

Just Accepted

$$\sigma_s = \begin{cases} E_{sc}(T, T_{\max}) \cdot \varepsilon_s & \varepsilon_s \le \varepsilon_{yc}(T, T_{\max}) \\ f_{yc}(T, T_{\max}) + 0.01 E_{sc}(T, T_{\max}) \varepsilon_s & \varepsilon_s > \varepsilon_{yp}(T, T_{\max}) \end{cases} \tag{3}$$

in which $f_{yc}(T, T_{\max})$, $\varepsilon_{yc}(T,\ T_{\max})$, $E_{sc}(T,\ T_{\max})$ represent the yield strength, yield strain, and elastic modulus of steel during the cooling stage, respectively.

$$f_{yc}(T, T_{\max}) = f_y(T_{\max}) - \frac{T_{\max} - T}{T_{\max} - T_0} \times [f_y(T_{\max}) - f_{yp}(T_{\max})] \tag{4}$$

$$\varepsilon_{yc}(T, T_{\max}) = \varepsilon_y(T_{\max}) - \frac{T_{\max} - T}{T_{\max} - T_0} \times [\varepsilon_y(T_{\max}) - \varepsilon_{yp}(T_{\max})] \tag{5}$$

$$E_{sc}(T, T_{\max}) = \frac{f_{yc}(T, T_{\max})}{\varepsilon_{yc}(T, T_{\max})} \tag{6}$$

For Grade 8.8 bolts, the evolution of mechanical properties during cooling follows the approach proposed by Hanus [17]. Considering the irreversible nature of thermal degradation, the yield strength of bolts during cooling is evaluated using Equation (7):

$$f_{yc}(T, T_{\max}) = k_b(T) \cdot k_{nr}(T, T_u) \cdot f_y(20°\mathrm{C}) \tag{7}$$

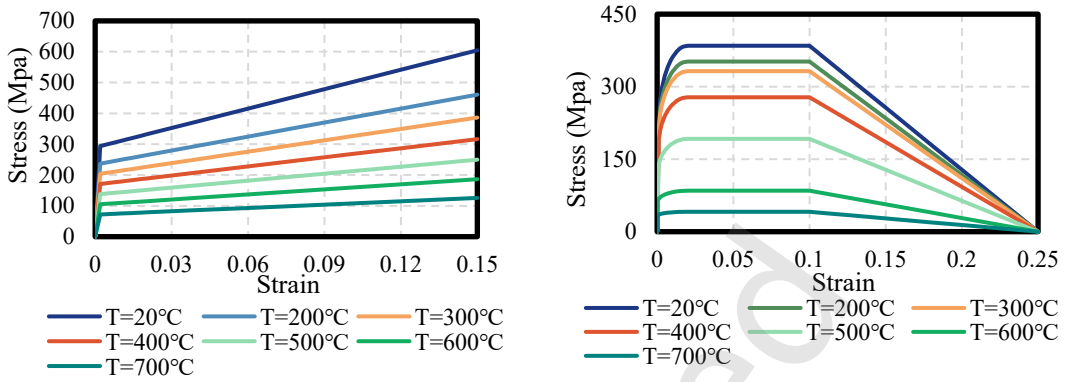
in which, $k_b(T)$ is the reduction factor specified in EN 1993-1-2 [18] , which accounts for strength degradation during heating but does not include cooling effects. The modified reduction factor incorporating cooling effects, $k_{nr}(T, T_u)$ is determined using Equation (8):

$$\begin{cases} k_{nr}(T, T_u) = 1 & T_{\max} \le 500°\mathrm{C} \\ k_{nr}(T, T_u) = 1 - 1.33 \times 10^{-3} \cdot (T_{\max} - \max(T_f, 500)) & 500°\mathrm{C} < T_{\max} \le 800°\mathrm{C} \end{cases} \tag{8}$$

The temperature-dependent stress–strain relationships for S355 structural steel and Grade 8.8 bolts are implemented in Abaqus. Two field variables are introduced: Field1 represents the current temperature, while Field2 records the maximum temperature previously experienced. During heating, Field1 and Field2 are identical. During cooling, Field1 follows the current temperature history, whereas Field2 retains the peak temperature reached at each integration point. A user-defined subroutine (VUSDFLD) is employed to update these variables and assign the corresponding material properties based on the thermal history. Figures 2 (a) and (b) show the stress–strain relationships of S355 steel and Grade 8.8 bolts during cooling after exposure to a peak temperature of 800 °C. The results indicate that the cooling-stage stress–strain response is

Just Accepted

governed by both the current temperature and the previously attained maximum temperature, reflecting irreversible high-temperature degradation.



(a) Stress-strain curves of steel at cooling stage (b) Stress-strain curves of bolt at cooling stage

Figure 2. Mechanical properties at cooling stage (T_{max} =800℃)

3.3 Temperature curves of beams and connections

Two thermal scenarios are considered for all beam–connection models. In the first scenario, a uniform temperature distribution is assumed across the beam section. In the second scenario, a temperature gradient is introduced through the beam depth to account for thermal bowing and to evaluate its influence on connection behaviour.

3.3.1 Calculation of beam and connections temperature

The beams and connections are assumed to be unprotected. Their temperature evolution is evaluated using the simplified heat transfer model specified in EN 1993-1-2 [18], as given in Equation (9):

$$\Delta\theta_{a,t} = K_{sh}\frac{A_m / V}{C_a \rho_a}\dot{h}_{net}\,\Delta t \tag{9}$$

In this formulation, A_m / V is the section factor, defined as the ratio of exposed surface area to volume; c_a and ρ_a are the specific heat and density of steel, respectively; Δt is the time increment; and $\dot{h}_{net}$ is the net heat flux per unit area acting on the steel surface. The net heat flux consists of convective and radiative components and is evaluated in accordance with EN 1993-1-2:2005 [19].

Just Accepted

For the uniform temperature assumption, a single section factor is calculated for the entire cross-section of the beam or connection. The corresponding temperature–time curve, obtained from the Eurocode formulation, represents the average temperature history of the member. For the non-uniform temperature assumption, a component-based approach is adopted to capture temperature gradients within the section. The beam cross-section is divided into the top flange, web, and bottom flange, and the section factor of each component is calculated individually based on its exposed surface area and volume. This results in distinct temperature–time curves for different regions of the beam. For the connection region, the temperature distribution under the non-uniform assumption is determined following the method proposed by Dai et al. [20]. The section factors of individual connection components are evaluated according to their actual geometrical configuration and exposure conditions. In the present study, separate section factors are calculated for the semi-elliptical ductile components, angle cleats, and flange cover plates.

Based on these component-level calculations, the temperature distribution within the connection is further described using the simplified analytical expressions proposed in this study, as given in Equations (10) – (13). The physical meaning of the parameters is illustrated in Figure 3. Accordingly, distinct temperature–time curves are obtained for the three connection configurations under both uniform and non-uniform temperature assumptions, as shown in Figure 4-Figure 6. These temperature histories are subsequently applied as predefined temperature fields in the finite element models to simulate the mechanical response of the connections throughout the entire fire process.

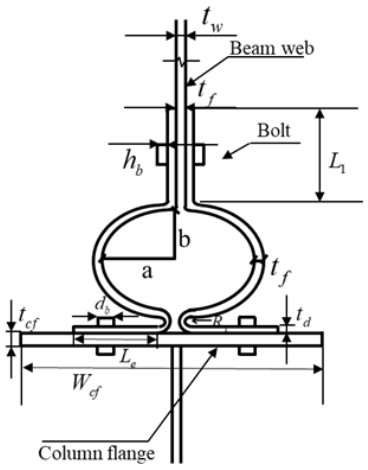
$$\frac{A_m}{V}=\frac{2\times[W_{cf}+t_{cf}+t_d+t_f+L_e+L_1+\pi R_1+\frac{2\pi \mathrm{b}+4(a-b)}{2}]+t_w}{W_{cf}\times t_{cf}+2\times(L_1t_f+L_et_d)+\pi[(a+t_f)(b+t_f)-ab]} \tag{10}$$

$$\frac{A_m}{V}=\frac{2\times(L_{a1}+W_{cf}+t_{cf})}{2\times(L_{a1}-t_a+L_b)\times t_a+W_{cf}\times t_{cf}+L_{a2}\times t_w} \tag{11}$$

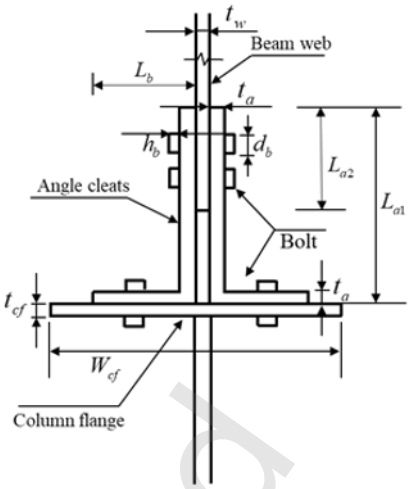
$$\frac{A_m}{V}=\frac{2\times[W_{cf}+t_{cf}+2L_{c1}+\pi b+2(a-b)+t_f]-t_w}{W_{cf}\times t_{cf}+4\times L_1\times t_f+2\times L_{c1}\times t_w+\pi(a+t_c)(b+t_c)-ab} \tag{12}$$

$$\frac{A_m}{V}=\frac{2\times(L_1+W_{cf}+t_{cf})+4t_p-t_w}{W_{cf}\times t_{cf}+2\times t_p\times L_2+t_w\times(L_2-L_0+L_1-L_2)} \tag{13}$$

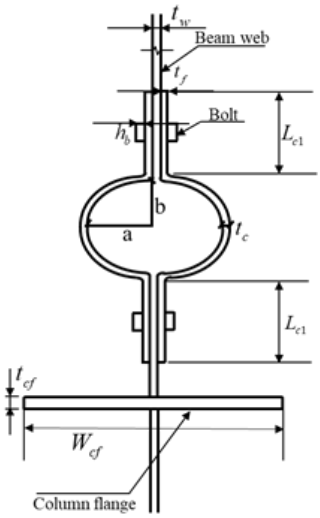
Just Accepted



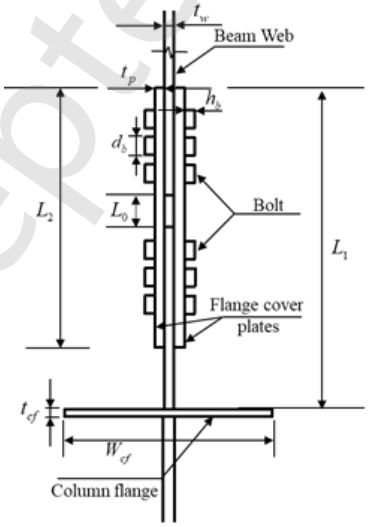
(a) Ductile component (for Prototypes 1 and 2)



(b) Angle cleat

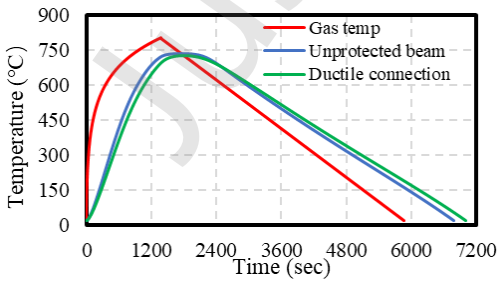


(c) Ductile component (for Prototype 3)

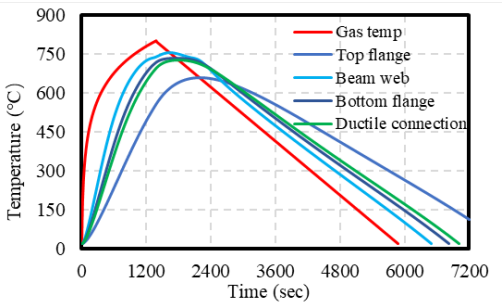


(d) Flange cover plate

Figure 3. Calculation of section factors for different connection components



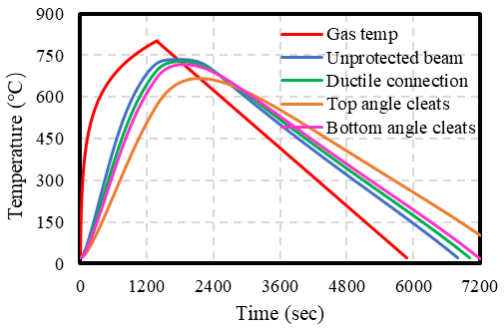
(a) Uniform temperature distribution in the beam



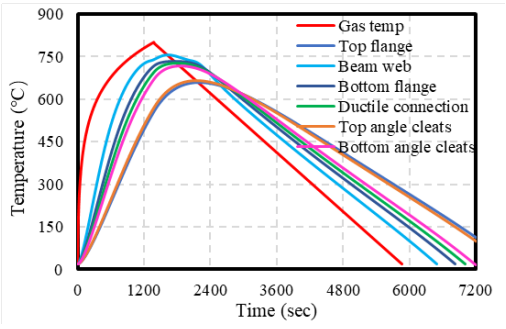
(b) Non-uniform temperature distribution in the beam

Figure 4. Temperature–time curves of the model (Prototype 1)

Just Accepted

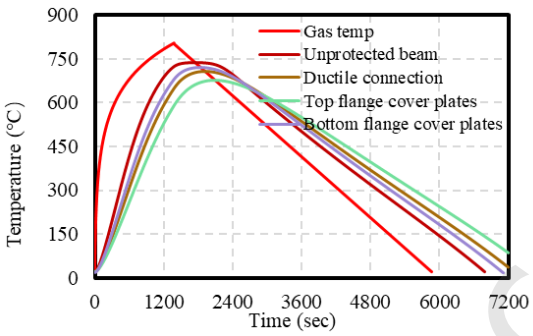


(a) Uniform temperature distribution in the beam

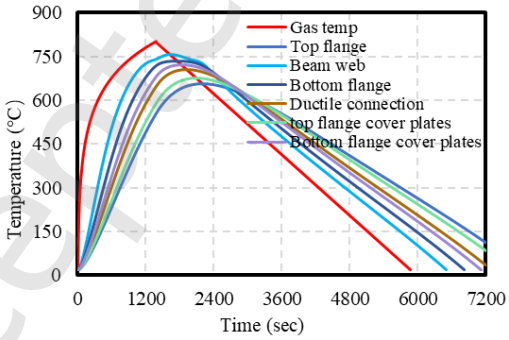


(b) Non-uniform temperature distribution in the beam

Figure 5. Temperature–time curves of the model (Prototype 2)



(a) Uniform temperature distribution in the beam



(b) Non-uniform temperature distribution in the beam

Figure 6. Temperature–time curves of the model (Prototype 3)

3.4 Simulation results

The mid-span deflection of the beam and the axial force in the connection (Figure 7-Figure 9) provide insight into the distinct mechanical responses of the three connection prototypes.

Prototype 1 exhibits a stable and gradual evolution of deformation throughout the entire thermal history. As shown in Figure 7 (a), the mid-span deflection develops smoothly, without abrupt changes during either the heating or cooling phases. A similar trend is observed in the axial force (Figure 7 (b)), which evolves in a controlled and progressive manner. This behaviour indicates that the semi-elliptical ductile components effectively accommodate tensile deformation throughout the fire process. Through distributed deformation, these components relieve the additional internal forces induced by restrained thermal expansion and subsequent catenary action, resulting in a stable and well-regulated force transfer mechanism.

Just Accepted

With the introduction of angle cleats, Prototype 2 exhibits increased initial stiffness, leading to a slightly reduced mid-span deflection during the early heating stage compared with Prototype 1 (Figure 8 (a)). However, as temperature increases and the structural response transitions towards catenary action, the deformation demand becomes less effectively distributed. Consequently, the axial force develops more rapidly (Figure 8 (b)), particularly at elevated temperatures. This indicates that the increased stiffness constrains the participation of the ductile components, thereby reducing the efficiency of force redistribution.

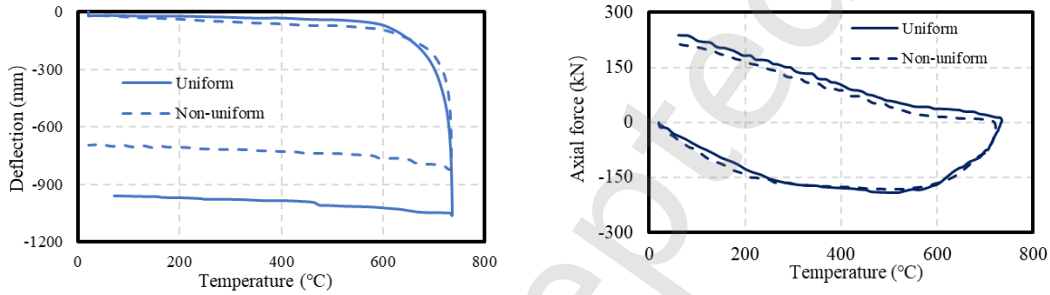
Prototype 3, incorporating flange cover plates, provides the highest level of stiffness and restraint. As shown in Figure 9 (a), beam-end rotation is significantly restrained during the heating phase, resulting in smaller deflection. However, this strong restraint leads to a continuous accumulation of axial force with increasing temperature (Figure 9 (b)). During the cooling phase, the tensile force further intensifies, accompanied by more localised deformation within the connection region, indicating a concentration of deformation and reduced redistribution capacity.

A comparison between the uniform and non-uniform temperature scenarios shows that the non-uniform temperature distribution modifies the deflection path and the timing of the compression-to-tension transition, rather than consistently increasing the final mid-span deflection. Although the evolution of axial force becomes more complex under non-uniform temperature distribution, the relative trends among the three prototypes remain consistent. The evolution of axial force clearly reflects the transition of structural behaviour during fire. At the initial heating stage, compressive axial force develops due to restrained thermal expansion. As temperature increases and beam stiffness degrades, the structural response gradually shifts towards catenary action, leading to a transition from compression to tension. This transition occurs smoothly in all three prototypes, demonstrating that the presence of ductile components ensures stable load transfer without sudden strength degradation. Under non-uniform temperature distribution, the temperature gradient across the beam section accelerates the development of catenary action, resulting in an earlier compression-to-tension transition and a moderately higher tensile force level. Although the axial force evolution becomes more complex, the relative behavioural characteristics of the three prototypes remain consistent.

Rather than indicating a simple performance hierarchy, the results reveal a clear shift in structural response governed by connection stiffness. Prototype 1 enables extensive participation of the

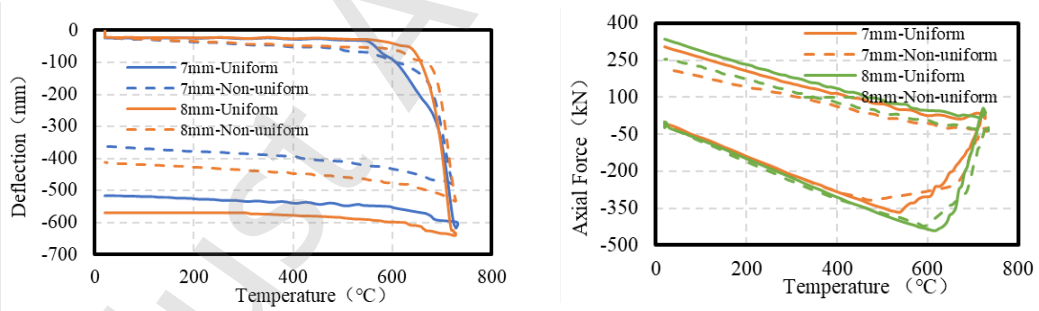
Just Accepted

ductile components, resulting in distributed deformation and effective force regulation. Prototype 2 represents an intermediate condition, where increased stiffness partially limits deformation redistribution. Prototype 3 is dominated by stiffness and restraint, leading to more concentrated force transfer and higher tensile force demand. These findings demonstrate that, although all three configurations incorporate ductile components and maintain stable behaviour throughout the fire process, the degree of stiffness plays a critical role in controlling deformation patterns, force redistribution, and the development of catenary action.



(a) Mid-span deflection of the beam (b) Axial force of the connection

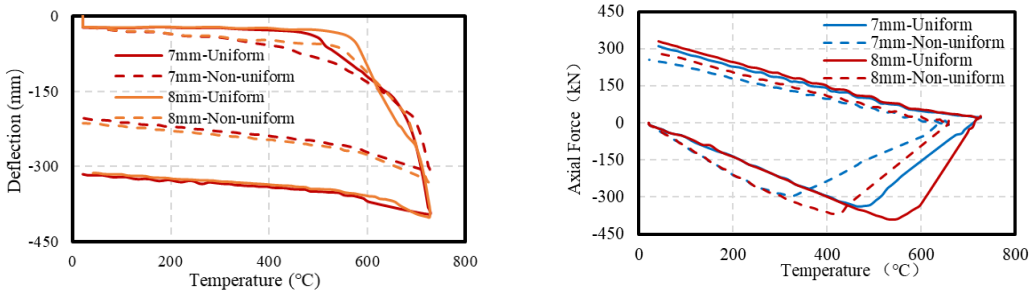
Figure 7. Numerical results of the beam under uniform and non-uniform temperature assumptions (Prototype 1)



(a) Mid-span deflection of the beam (b) Axial force of the connection

Figure 8. Numerical results of the beam under uniform and non-uniform temperature assumptions (Prototype 2)

Just Accepted



(a) Mid-span deflection of the beam (b) Axial force of the connection

Figure 9. Numerical results of the beam under uniform and non-uniform temperature assumptions (Prototype 3)

4. Performance of connections under earthquake conditions

4.1 Numerical modelling in Abaqus

Finite element models were developed in Abaqus to investigate the seismic performance of the proposed ductile connections. The geometric configurations of Prototypes 1–3 are identical to those adopted in the fire analysis (Section 3.1). Detailed dimensions are therefore not repeated here and can be found in Table 1.

In the fire analysis, a dynamic explicit step was employed, in which temperature effects were introduced via predefined temperature fields assigned according to the calculated temperature–time histories. This approach enables the incorporation of temperature-dependent material degradation without the need for fully coupled thermo-mechanical analysis. In contrast, the seismic analysis was conducted using a static general step under ambient temperature conditions. No thermal fields were applied. The material properties of S355 structural steel and Grade 8.8 bolts are consistent with those adopted in the fire analysis at room temperature. In addition, bolt pretension was explicitly included to represent the actual assembly condition of high-strength bolted connections.

To accurately capture cyclic behaviour, the mesh density and boundary conditions were refined according to the loading configuration. These modelling strategies ensure consistency in geometry and baseline material definitions between the fire and seismic analyses, while appropriately reflecting the distinct physical mechanisms governing high-temperature response and cyclic plasticity. The cyclic loading protocol adopted in the seismic analysis is described in Section 4.2, and the corresponding numerical results are presented in Section 4.3.

Just Accepted

4.2 Loading protocol

A displacement-controlled loading scheme was adopted to evaluate the cyclic performance of the proposed ductile connections. The loading protocol follows the recommendations of ATC-24 [21], which is widely used for cyclic testing of steel structural components.

The loading process is divided into three stages: elastic, yielding, and post-yield (ultimate). The reference displacement amplitude is defined based on the yield displacement, Δ_y, obtained from the monotonic response of the connection. In the elastic stage, each displacement amplitude is applied for two fully reversed cycles. At the yielding stage, each displacement level is repeated for three cycles to capture stable hysteretic behaviour. In the post-yield stage, each displacement amplitude is imposed for two cycles until significant strength degradation or instability occurs. The detailed loading history adopted for the ductile connections is illustrated in Figure 10.

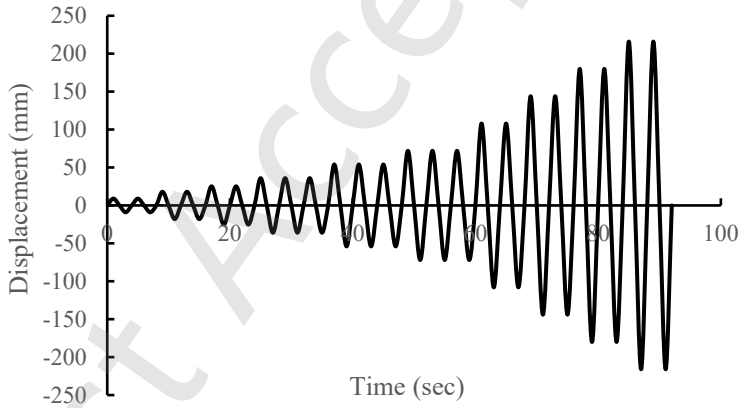


Figure 10. Loading system of the ductile connection

4.3 Simulation results

Figure 11 presents the moment–rotation hysteretic responses of the three connection prototypes under cyclic loading. All configurations develop stable and closed hysteresis loops that progressively expand with increasing loading amplitude. No abrupt strength degradation or instability is observed, indicating reliable load-carrying capacity and energy dissipation throughout the loading history.

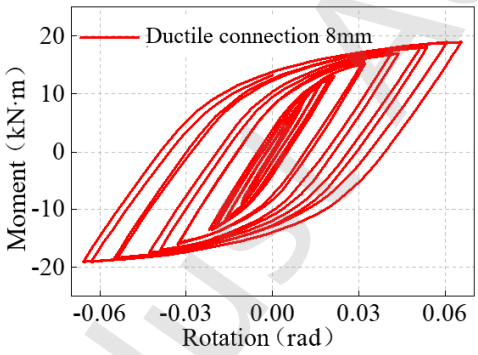
Clear differences in hysteretic behaviour are observed among the three configurations. Prototype 1 exhibits a relatively low moment capacity (approximately ±20 kN·m) but a significantly larger rotation capacity (up to approximately ±0.06 rad). The hysteresis loops are slender and stable, with

Just Accepted

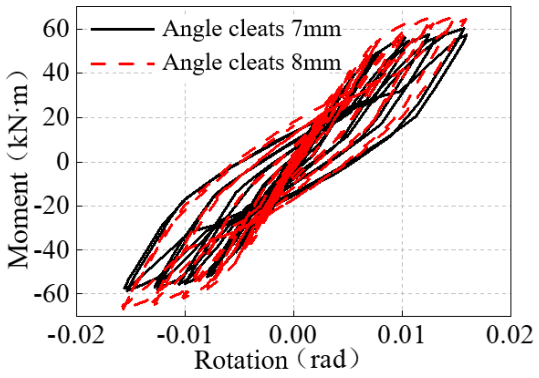
smooth loading and unloading paths and no evident pinching. The loops remain well-developed under repeated cycles, indicating effective plastic deformation development and stable force transfer. This behaviour demonstrates excellent ductility and deformation compatibility, consistent with a rotation-dominated response.

Prototype 2 shows an increased moment capacity (approximately ±60 kN·m) with a reduced rotation capacity (approximately ±0.016 rad). The hysteresis loops become fuller, while a moderate pinching effect is observed near the zero-rotation region, suggesting the occurrence of connection slip or localised nonlinear deformation. In addition, stiffness degradation becomes evident with increasing cycles. This behaviour is characteristic of semi-rigid connections, where both moment resistance and deformation capacity contribute to the response.

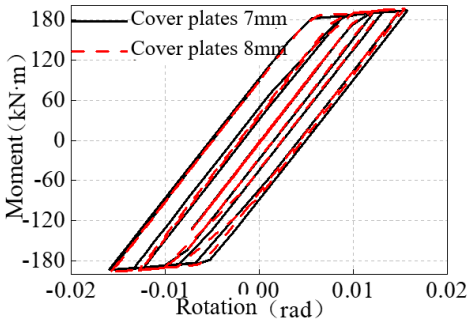
Prototype 3 exhibits the highest stiffness and load-carrying capacity, with moment amplitudes reaching approximately ±190 kN·m and a rotation capacity of about ±0.015 rad. The hysteresis loops are regular and stable, with nearly parallel loading and unloading branches and no obvious pinching effect. This indicates a stiffness-dominated response, in which moment transfer governs the connection behaviour.



(a) Prototype 1



(b) Prototype 2



Just Accepted

(c) Prototype 3

Figure 11. Moment–rotation hysteretic responses of the three connection prototypes

Figure 12 presents the corresponding moment–rotation backbone curves derived from the hysteretic responses shown in Figure 11, providing a clearer comparison of the global mechanical characteristics of the three connection prototypes.

Consistent with the hysteretic behaviour, the three prototypes exhibit distinctly different moment–rotation relationships. Prototype 1 is characterised by a relatively low moment capacity but a significantly larger rotation range, indicating a deformation-dominated response. The backbone curve develops smoothly without noticeable strength degradation, confirming that the ductile components can sustain stable deformation while maintaining load transfer. This behaviour is consistent with a pinned-type response, but with enhanced stability due to the continuous participation of the ductile elements.

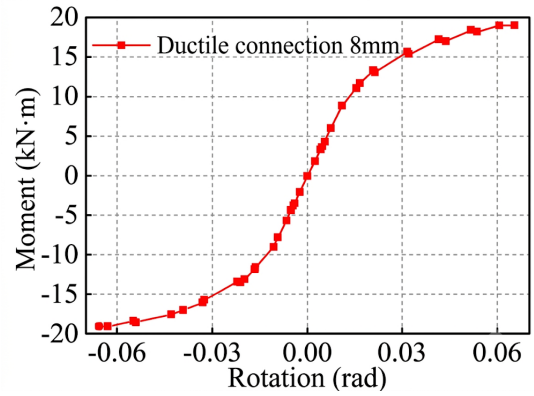
Prototype 2 demonstrates an intermediate response, with a clear increase in moment capacity accompanied by a reduction in rotation capacity. The backbone curves show a gradual transition from the initial elastic stage to the nonlinear range, followed by moderate stiffness degradation at larger rotations. This reflects a semi-rigid behaviour, where both the angle cleats and the ductile components contribute to the overall response. The connection is able to balance strength and deformability, although the deformation capacity is partially constrained compared with Prototype 1.

Prototype 3 exhibits a steep initial slope and the highest moment capacity, while its rotation capacity remains relatively limited. The backbone curves are nearly linear over a wide range, indicating that the connection response is dominated by stiffness and moment transfer. This behaviour is characteristic of rigid connections, where deformation is more localised and global rotation is restricted.

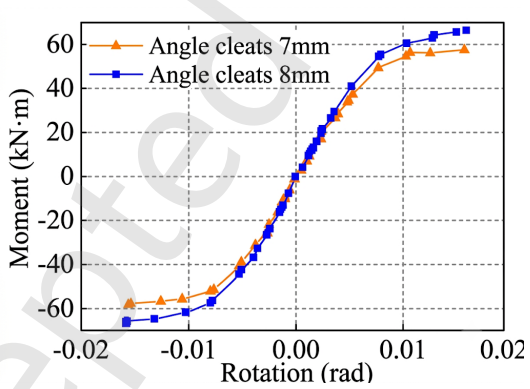
For Prototypes 2 and 3, minor differences can be observed between the curves corresponding to different component thicknesses; however, these variations mainly affect the magnitude of moment resistance and do not alter the overall shape or fundamental behaviour of the curves. This further confirms that the global response of the connections is governed primarily by their configuration and load-transfer mechanism, rather than by local geometric variations.

Just Accepted

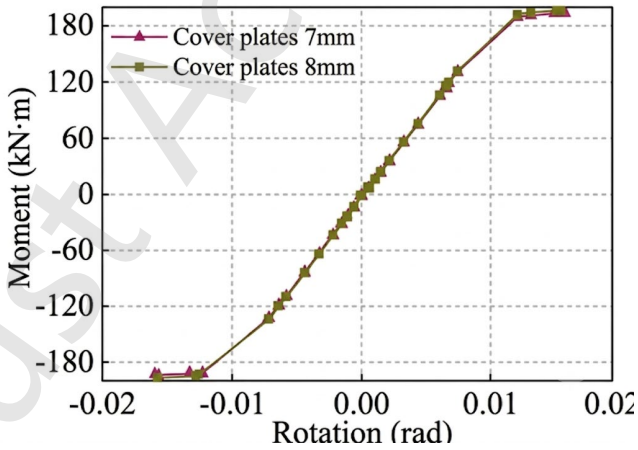
Overall, the backbone curves clearly demonstrate a progressive transition in structural behaviour from deformation-dominated (Prototype 1), through balanced performance (Prototype 2), to strength-dominated response (Prototype 3). Importantly, all three configurations exhibit smooth and continuous responses without abrupt strength loss, indicating that the incorporation of ductile components effectively stabilises the mechanical behaviour and ensures reliable performance under cyclic loading.



(a) Prototype 1



(b) Prototype 2



(c) Prototype 3

Figure 12. Moment–rotation back bone curves of the three connection prototypes

5. Conclusions

This study presents a comprehensive investigation of three novel beam–column connection prototypes incorporating semi-elliptical ductile components under both fire and seismic loading conditions. Based on the numerical analyses, the following conclusions can be drawn:

(1) All three connection prototypes exhibit stable mechanical behaviour throughout the entire fire

Just Accepted

process, including heating and cooling stages. The presence of ductile components ensures smooth load transfer and prevents abrupt strength degradation under varying thermal conditions.

(2) The evolution of axial force reveals a clear transition from compression, induced by restrained thermal expansion, to tension governed by catenary action at elevated temperatures. During the cooling phase, tensile forces may further increase due to the partial recovery of material stiffness. This transition occurs in a stable and controlled manner in all prototypes, demonstrating the effectiveness of the ductile components in accommodating large deformation demands.

(3) Connection stiffness plays a key role in governing structural response. Prototype 1 promotes distributed deformation and efficient force regulation, Prototype 2 represents an intermediate condition with balanced stiffness and deformability, and Prototype 3 exhibits a stiffness-dominated response with higher force concentration and reduced deformation redistribution capacity.

(4) Under cyclic loading, all prototypes exhibit stable cyclic responses, while their energy dissipation capacities differ significantly. Prototype 1 provides the largest deformation capacity, Prototype 2 shows balanced strength and ductility, and Prototype 3 is mainly stiffness- and strength-dominated with relatively limited rotational ductility.. Plastic deformation is primarily concentrated within the ductile components, confirming their role as structural fuses that protect the primary structural members.

(5) The results demonstrate that the global behaviour of the connections is governed by the interaction between stiffness and deformability. While increased stiffness enhances load-carrying capacity, it may limit deformation redistribution and lead to higher force concentration.

Overall, the proposed ductile connection system effectively integrates controlled plastic deformation and stable force redistribution under both fire and seismic actions. This provides an efficient strategy for improving the robustness, adaptability, and multi-hazard resilience of steel beam–column connections.

Acknowledgements

The authors gratefully acknowledge the financial support of the National Natural Science Foundation of China (52208489), and the Shanghai Pujiang Program (22PJ1411500).

Author contribution statement

Just Accepted

"Author 1 is responsible for Work 1. …All the authors have approved the final manuscript." CRediT author statement (https://credit.niso.org/) is recommended to use, and all the listed authors should meet the definition of Author in ICMJE recommendations (https://www.icmje.org/).

Data availability

"Not applicable."

OR "The data that support the findings of this study could be downloaded from xxxxxxx / is available from the corresponding author upon reasonable request."

Use of AI statement

"None."

OR "During the preparation of this work, the author(s) used [NAME TOOL / SERVICE] in order to [REASON]. After using this tool/service, the author(s) reviewed and edited the content as needed and take(s) full responsibility for the content of the publication."

Declaration of competing interest

The author(s) have no competing interests to declare that are relevant to the content of this article.

REFERENCES

[1] T. McAllister, G. Corley, World Trade Center Building performance study: Data collection, preliminary observations, and recommendations, Federal Emergency Management Agency2002.
[2] T. Lennon, D. Moore, The natural fire safety concept—full-scale tests at Cardington, Fire Safety Journal 38(7) (2003) 623-643.
[3] Y. Liu, S.-S. Huang, I. Burgess, Investigation of a steel connection to accommodate ductility demand of beams in fire, Journal of Constructional Steel Research 157 (2019) 182-197.
[4] Y. Liu, S.-S. Huang, I. Burgess, Component-based modelling of a novel ductile steel connection, Engineering Structures 208 (2020) 110320.
[5] Y. Liu, S.-S. Huang, I. Burgess, Performance of a novel ductile connection in steel-framed structures under fire conditions, Journal of Constructional Steel Research 169 (2020) 106034.
[6] Y. Liu, S.-S. Huang, I. Burgess, Fire performance of axially ductile connections in composite construction Fire Safety Journal (2021) 103311.
[7] Y. Liu, S.-S. Huang, I. Burgess, Three-dimensional modelling of composite frames with ductile connections in fire, Structures, Elsevier, 2022, pp. 665-677.
[8] Y. Wang, H. Zhou, Y. Shi, H. Chen, Research status of brittle fracture in steel frame beam-column joints under seismic action, Proceedings of the 11th National Conference on Modern Structural Engineering and the Celebration of the 60th Anniversary of Professor Liu Xiliang's Teaching Career (2011).
[9] X. He, Y. Chen, M.R. Eatherton, T. Shao, Experimental evaluation of replaceable energy dissipation connection for moment-resisting composite steel frames, Journal of Structural

Just Accepted

Engineering 144(6) (2018) 04018042.
[10] H. Tagawa, Y. Nagoya, X. Chen, Bolted beam-to-column connection with buckling-restrained round steel bar dampers, Journal of Constructional Steel Research 169 (2020) 106036.
[11] M. Wang, P. Bi, Study on seismic behavior and design method of dissipative bolted joint for steel frame with replaceable low yield point steel connected components, Construction and Building Materials 198 (2019) 677-695.
[12] D. Pantousa, T.L. Karavasilis, Numerical assessment of the fire behavior of steel posttensioned moment-resisting frames, Journal of Structural Engineering 146(4) (2020) 04020032.
[13] T. Golea, A.F. Santos, J.-P. Jaspart, M. Latour, A. Santiago, J.-F. Demonceau, Design for robustness of steel structures with dissipative FREEDAM joints, Ingegneria Sismica (2) (2022).
[14] Y. Liu, S.-S. Huang, I. Burgess, B. Peng, Optimization of Failure Modes of a Ductile Connection Under Fire Conditions, Fire Technology (2024).
[15] L.-H. Han, H. Yang, S.-L. Cheng, Residual strength of concrete filled RHS stub columns after exposure to high temperatures, Advances in Structural Engineering 5(2) (2002) 123-134.
[16] H. Yang, L.-H. Han, Y.-C. Wang, Effects of heating and loading histories on post-fire cooling behaviour of concrete-filled steel tubular columns, Journal of Constructional Steel Research 64(5) (2008) 556-570.
[17] F. Hanus, G. Zilli, J.-M. Franssen, Behaviour of Grade 8.8 bolts under natural fire conditions—Tests and model, Journal of Constructional Steel Research 67(8) (2011) 1292-1298.
[18] CEN, Eurocode 3: Design of steel structures - Part 1–2: General rules—Structural fire design. BS EN 1993-1-2: 2005, 2005.
[19] <EN.1993.1.2.2005.pdf>.
[20] X. Dai, Y. Wang, C. Bailey, A Simple Method to Predict Temperatures in Steel Joints with Partial Intumescent Coating Fire Protection, Fire Technology 46(1) (2010) 19-35.
[21] H. Krawinkler, A.T. Council, A. Iron, S. Institute, A.I.o.S. Construction, N.C.f.E.E. Research, N.S. Foundation, Guidelines for Cyclic Seismic Testing of Components of Steel Structures, Applied Technology Council1992.

Just Accepted